



# MIT Open Access Articles

## *Fabrication and Characterization of Folded Foils Supporting Streamwise Traveling Waves*

The MIT Faculty has made this article openly available. **Please share** how this access benefits you. Your story matters.

<b>Citation</b>	Calisch, S, Gershenfeld, N, Fan, D, Jodin, G and Triantafyllou, M. 2021. "Fabrication and Characterization of Folded Foils Supporting Streamwise Traveling Waves." 147.
<b>As Published</b>	10.1007/978-3-030-55594-8_33
<b>Publisher</b>	Springer International Publishing
<b>Version</b>	Author's final manuscript
<b>Citable link</b>	<a href="https://hdl.handle.net/1721.1/137159">https://hdl.handle.net/1721.1/137159</a>
<b>Terms of Use</b>	Creative Commons Attribution-Noncommercial-Share Alike
<b>Detailed Terms</b>	<a href="http://creativecommons.org/licenses/by-nc-sa/4.0/">http://creativecommons.org/licenses/by-nc-sa/4.0/</a>

# FABRICATION AND CHARACTERIZATION OF FOLDED FOILS SUPPORTING STREAMWISE TRAVELING WAVES

Sam Calisch<sup>1</sup>, Neil Gershenfeld<sup>1</sup>, Dixia Fan<sup>2</sup>, Gurvan Jodin<sup>2,3</sup>, Michael Triantafyllou<sup>2</sup>

<sup>1</sup>*Center for Bits and Atoms, Massachusetts Institute of Technology  
Cambridge, MA, USA*

<sup>2</sup>*Department of Ocean Engineering, Massachusetts Institute of Technology  
Cambridge, MA, USA*

<sup>3</sup>*LAPLACE and IMFT, Université de Toulouse, CNRS  
Toulouse, France*

## Abstract

A body of work has grown around the use of small amplitude traveling waves on aerodynamic and hydrodynamic surfaces for boundary layer control. In particular, when the traveling wave speed exceeds the free stream velocity, significant drag reductions have been shown in simulation. Building viable prototypes to test these hypotheses, however, has proven challenging. In this paper, we describe a candidate system for constructing structural airfoils and hydrofoils with embedded electromagnetic actuators for driving high velocity traveling waves. Our approach relies on the fabrication of planar substrates which are populated with electromagnetic components and then folded into a prescribed three dimensional structure with actuators embedded. We first specify performance characteristics based on hydrodynamic requirements. We then describe the fabrication of fiber-reinforced polymer composite substrates with prescribed folding patterns to dictate three dimensional shape. We detail the development of a miniaturized single-phase linear motor which is compatible with this approach. Finally, we compare the predicted and measured force produced by these linear motors and plot trajectories for a 200 Hz driving frequency.

**Keywords:** traveling waves, separation control, distributed actuation, origami.

## 1 Introduction

Both computational and experimental work has grown around the use of small amplitude traveling waves on aerodynamic or hydrodynamic surfaces for boundary layer control and drag reduction. This work has demonstrated significant drag reductions over a wide range of Reynolds numbers so long as the wave speed moderately exceeds the free stream speed [5, 29, 32, 35–37]. In these cases, the energy required to drive the traveling waves can be made to be significantly less than the energy savings from drag reduction. Despite these results, fabricating viable high-speed traveling waves on aerodynamic surfaces remains a great challenge. This work investigates performance of structural systems with distributed aerodynamic actuation made using origami-inspired methods of cutting and folding fiber-reinforced composites. Such systems could be designed as airfoil sections, ship hulls, vehicle fairings, or automobile panels, potentially providing drag reduction and energy savings for these applications.

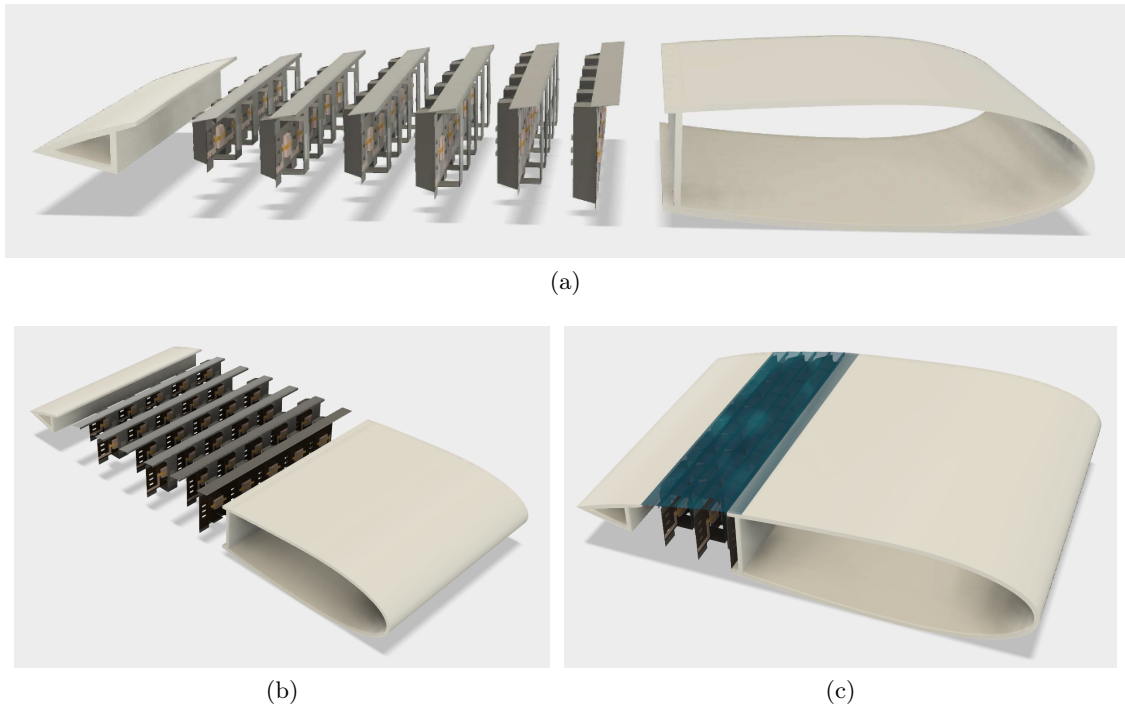


Figure 1: Traveling wave elements included near the  $3/4$  chord position of a foil. A) Exploded side view, B) Exploded perspective view, C) Assembled perspective view.

Origami-inspired fabrication methods have enjoyed considerable success in micro-robotics, where the scale of actuators and assemblies prevents manual assembly [34]. These techniques leverage CNC fabrication and lamination techniques similar to those used in printed circuit board manufacturing. Typically a sequence of cutting, consolidation, and curing steps is used to produce a laminate with fiber-reinforced members joined by flexible hinge elements with integrated actuation and electrical interconnect. Micro-robots produced this way have been shown operable at hundreds of hertz [17], and capable of using a variety of actuation (e.g. piezoelectric [14], dielectric elastomer [6], electromagnetic [11], shape memory alloy [9], and fluidic [16]) and sensing [1, 2, 15, 30, 31] technologies. Further, the folding mechanisms specified by hinge patterns not only create effective transmissions for motion [20] and be made self-folding [8], but also can be used to simplify delicate three dimensional assembly tasks [18, 23, 24] to repeatably produce robots with minimal manual assembly.

Origami-inspired methods have also been used at a larger scale to create high-performance structural materials. Honeycombs like those used in lightweight sandwich panels can be directly produced with a specified three-dimensional shape by simply specifying a pattern of two-dimensional cuts and folds [22, 28], thus avoiding costly and imprecise machining of honeycombs. This construction has shown potential for scalable production [4, 33], and related constructions have already been demonstrated at commercial scales [12, 25–27]. Further, folding mechanics can be used to tailor material properties [3, 7, 10, 21] over a range of mechanical performance.

This work seeks to leverage these two bodies of work to address the challenge of constructing high-performance structural systems with distributed actuation of traveling surface waves. In what follows, we first characterize the desired performance of a distributed actuation system based on hydrodynamic arguments. We then de-

tail our construction approach, starting with the fabrication of a fiber-reinforced substrate with prescribed hinge lines. We then describe the development of an electromagnetic linear motor which functions when its components are populated onto the substrate, and outline assembly steps for a complete system prototype. Finally, we compare measured forces with simulation and verify high frequency operation.

## 2 Fluid mechanical actuation specifications

We begin by developing a set of specifications for a distributed actuation system for driving traveling waves on a hydrodynamic surface. For the characteristics of a desired wave shape, we reference the study of Shen et al. [29] for Reynolds number  $Re = U\lambda/\nu \approx 10^4$ . We use three parameters to specify the wave shape: the amplitude  $a$ , the wavelength  $\lambda$  and the wall motion phase speed  $c$ . The actuation frequency  $f$  of the actuators is derived as  $f = c/\lambda$ .

The literature uses the wave number ( $k = 2\pi/\lambda$ ) times the amplitude to specify the wave steepness. Studies suggest values of  $ka$  of the order of 0.2 are appropriate. The wave speed is similarly prescribed by the dimensionless ratio  $c/U$ , where  $U$  is the free stream flow velocity. When this ratio is made greater than 1, separation is eliminated and the wall waves generate a thrust. At  $c/U \approx 1.2$ , energy optimality has been observed, as the power required to actuate the wall plus the power saved due to drag reduction is minimal. The choice of the wavelength is a tradeoff between actuator manufacturing constraints and fluid mechanic considerations.

To satisfy values from the literature and be within the constraints of a feasible actuator to design, we select an amplitude  $a = 1mm$ , a wavelength  $\lambda = 20mm$ , and frequency  $f = 60Hz$ . This gives a wave steepness of .314 and allocates four actuators per wavelength if each requires  $5mm$  of chordwise extent. With a freestream velocity  $U \approx 1m/s$  and a chord of  $0.15m$ , this gives  $c/U \approx 1.2$  and chordwise  $Re \approx 7.5 \times 10^4$ .

To estimate the force requirements, we consider only force normal to the wall and assume a worst case estimate of actuating the suction side with maximal acceleration under the maximum pressure and inertial forces. Assuming a hexagonal packing of actuators with half-cell-span of  $5mm$  as above, each actuator is responsible for a surface patch of area  $A = 100mm^2$ . Numerical simulation provides a pressure coefficient of 0.06, leading to  $30Pa$  pressure. A typical hydrodynamic pressure is around  $500Pa$ . The total force produced by these pressures is around  $53mN$ .

To calculate the inertial forces, we must consider the actuator inertia and the fluid added mass. In general, the added mass in such a case of connected moving walls is not constant. In the case where the region under consideration has a small chordwise extent relative to  $\lambda$ , the force due to added mass can be written as  $F = \rho akA(c-U)^2$ . For the parameters identified above, this added mass force is on the order of  $1mN$  (but increases greatly at larger values of  $c/U$ ). Assuming a moving mass of  $100mg$ , the total required inertial force to operate at  $60Hz$  is roughly  $15mN$ . This gives a total force requirement of roughly  $70mN$ .

## 3 Construction

In this section we detail the design and fabrication of our candidate structural system with distributed actuation for traveling surface waves. We first show a method of producing stiff, fiber-reinforced composites with prescribed compliant hinge lines. We then describe a miniaturized, single-phase linear motor, suitable for embedding in a structure to produce traveling waves. Finally, we detail assembly

steps of this construction, showing how folding allows much of the work to be done in a flat state, making the process more repeatable and amenable to automation.

### 3.1 Composite construction

To fabricate fiber-reinforced composites with prescribed hinge lines, we use a method similar to one commonly used in microrobotics (c.f. [34]) where sheets of resin-impregnated carbon fiber are cut and then bonded to a polymer layer (often Kapton or PET). In regions where the fiber reinforcements have been removed, only the polymer layer remains, forming a compliant, robust hinge. Hinge cycle lifetimes approaching  $10^7$  have been shown in microrobotics applications with significant angular deflection, and an exponential relationship between hinge bending length and cycle life has been identified [19]. At larger scales where hinge lengths can be greater and angular deflections can be smaller, significantly increased lifetimes are expected and indefinite operation may be attained by staying below the material fatigue limit.

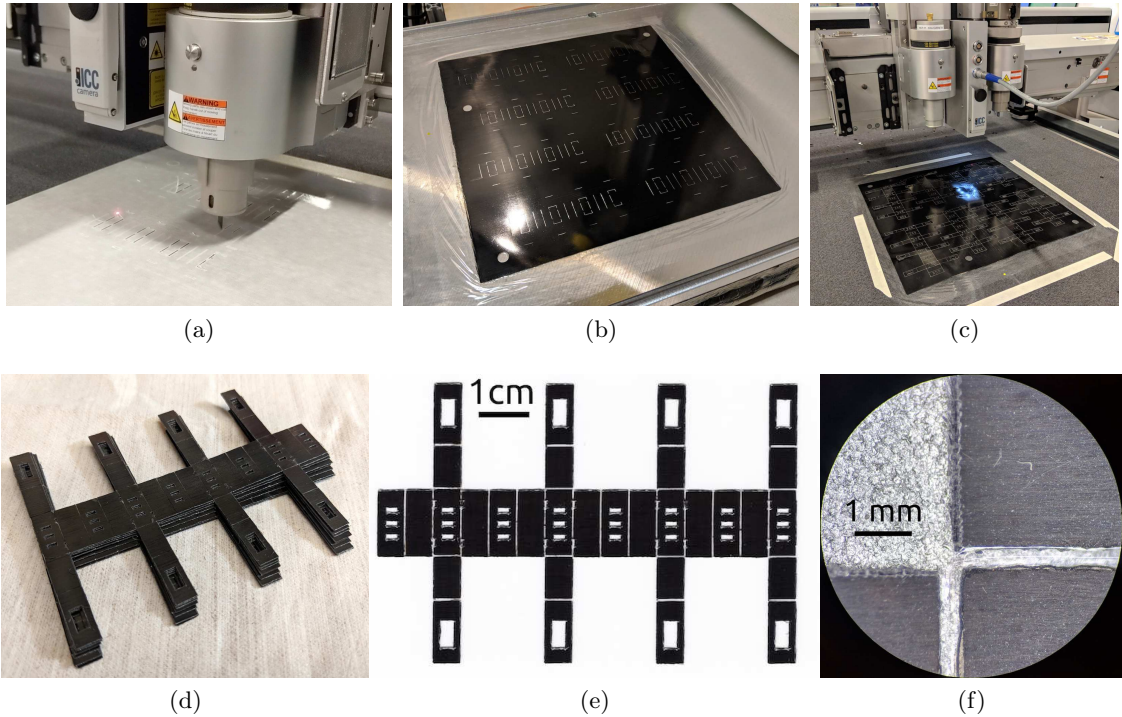


Figure 2: Fabrication of fiber-reinforced polymer composite laminates. A) Cutting resin-impregnated carbon fiber using oscillating knife to form hinges, B) Curing resin-impregnated carbon fiber between two sheets of 12 micron PET film, C) Optically registering and cutting cured laminate using oscillating knife, D) Batch of fiber-reinforced parts produced, E) Optical scan of part, showing clear hinges void of fiber reinforcement, F) Microscope image of two incident hinge lines.

Our fabrication process is shown in Figure 2. In Figure 2a, a stack of resin-impregnated carbon fiber layers is cut with an oscillating knife on a flatbed cutting machine. The stack consists of three layers of unidirectional carbon with a 0-90-0 layup schedule. This cutting step removes hinge lines with a width of approximately  $400\mu\text{m}$ . Next in Figure 2b, the carbon layer is placed between two sheets of  $12\mu\text{m}$  PET film and cured under a vacuum bag at  $200^\circ\text{C}$  for two hours. In Figure 2c, this cured laminate is optically registered on the flatbed cutting machine and cut



again using an oscillating knife to form registration features and an outline. The composite strips produced in one cycle are shown in Figure 2d. A scan of a single strip is shown in Figure 2e and a microscope image of two hinge lines is shown in Figure 2f. For this prototype, the finished thickness of carbon fiber layers was roughly 150 $\mu$ m, while the combined PET hinge layer thickness was 25 $\mu$ m.

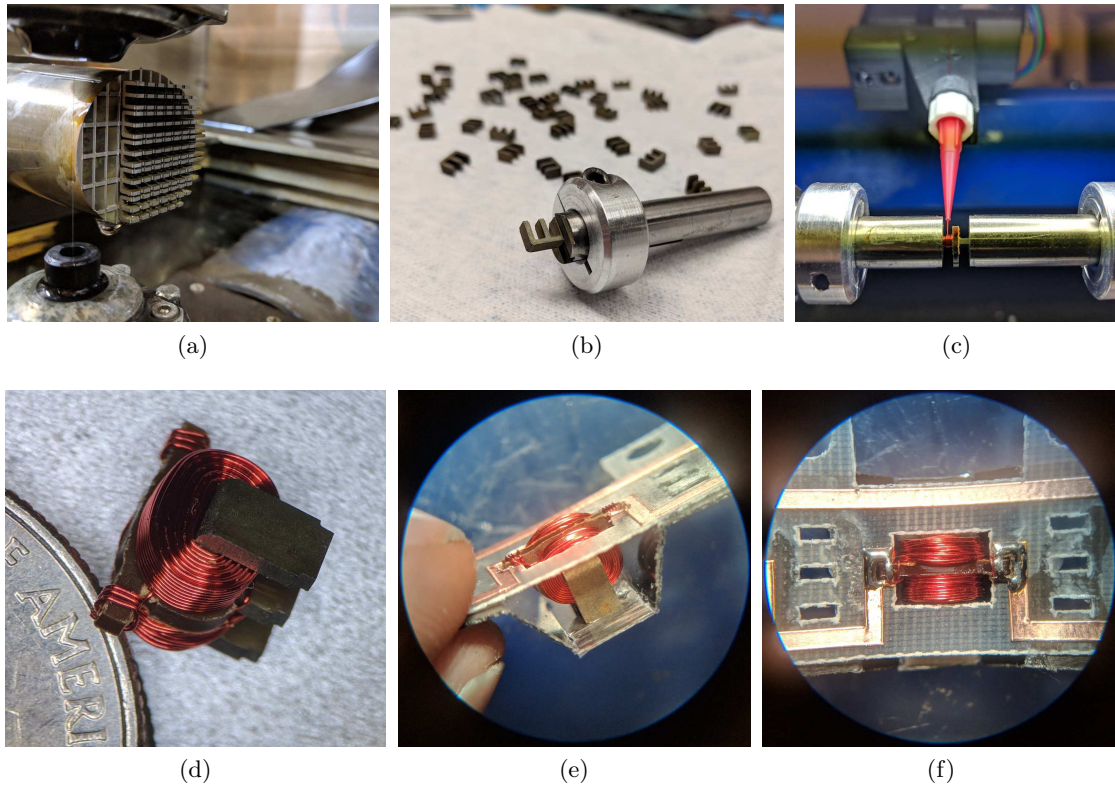


Figure 3: A) Electric discharge machining cores from round Vimvar stock, B) Released cores with winding clamp, C) Core during winding, D) Wound core with terminations (U.S. Quarter coin for scale), E) Wound core placed in honeycomb scaffolding, F) Wound core soldered for electrical connection.

In microrobotics applications, the polymer layer is usually sandwiched between two layers of fiber reinforcement to minimize its required bending radius. In larger scale applications with wider hinges, a single layer of fiber reinforcement can be sandwiched by two polymer layers. The wider hinge maintains safe polymer bending radii, and placing the continuous polymer layers outside of the fiber reinforcement layer makes the resulting structure more robust to delamination. As resin-impregnated carbon fiber sheets are usually available in substantially thicker dimensions than polymers like PET, this layer inversion allows for thinner resulting laminates. Finally, when a polymer is sandwiched by two fiber layers that have been precisely machined, alignment of these layers is tantamount. With a single machined fiber layer, no alignment is necessary, simplifying the fabrication process.

When assembled, the strip produced in Figure 2 will form one layer of a hexagonal-celled honeycomb with integrated actuators and flexure bearings (one of the units pictured in Figure 1a). The physical example produced here has a uniform size, and so the resulting honeycomb will have a constant thickness. To produce honeycombs

filling a desired shape, however, we can apply the geometric derivations of [4] or [28] to contour a given shape such as the foil shape shown in Figure 1.

### 3.2 Linear motors

To actuate the traveling waves, we now describe the design of a small, single phase linear motor ideal for embedding in folded structures. Linear motors often use three phases to extend actuation forces to large strokes, but because the required amplitudes for this application are only on the order of one millimeter, we use a single phase to simplify driving and wiring requirements and miniaturize the size of the actuator. As a large number of these actuators are required, we selected an "E" core shape which can be wound simply and fits inside a hexagonal honeycomb cell efficiently. Further, this core design can be parameterized easily to include any number  $N > 2$  of electrical poles, where the force produced scales linearly with the number of poles (assuming the number of magnetic poles is always  $N - 1$ ).

In Figure 3, we show the fabrication of these linear motors. First, in Figure 3a, core shapes are cut from round stock of Vimvar, a relatively inexpensive electrical iron with high permeability ( $\mu_r \approx 10,000$ ), high saturation induction ( $B_s \approx 2.1T$ ). Two wire cuts are made at 90 degrees from each other, enabling three dimensional features and producing many cores in a single machining operation. In Figure 3b, the produced magnetic cores are parted off and prepared for winding with 34 AWG magnet wire. A custom-built precision coil winder head is used to lay two opposing coils of 90 wraps each. The coil winder uses a Luer-Lok dispensing tip for accurate magnet wire placement and high packing density, shown in Figure 3c. The coil winding head allows the coils to be placed automatically, requiring operator intervention only when starting or finishing a coil. This significantly decreases the time required to wind a core and reduces error and inconsistencies in the actuator construction. The coils are heat-set using a hot air gun and the wire ends are terminated and wrapped around a central winding guide made of paper phenolic, shown in Figure 3d. These terminations can be tinned with a standard soldering iron and connected with the copper traces used in our construction, shown in Figures 3e and 3f.

These wound cores constitute the stator of our linear motor. The rotor consists of two Neodymium permanent magnets (N50, 3mm x 3mm x 0.5mm) magnetized through thickness and oriented with opposite polarity. A wedge of Vimvar acts as a backiron flux return for this magnet pair. When the phase is energized with current, magnetic flux is directed alternately in and out of the legs of the magnetic core. This produces a force on the rotor that seeks to align the field of produced by the permanent magnets with that of the magnetic core. By alternating the direction of current periodically, the rotor can be made to oscillate at the driving frequency.

### 3.3 Assembly

To create a functional unit, fiber-reinforced composite substrates and the magnetic components of the linear motor are combined in a set of assembly steps, shown in Figure 4. In Figure 4a, the wound magnetic cores, magnets, and back-iron components are populated on the composite substrate while in the flat state. This step is currently performed manually, but can be automated in much the same manner as industrial PCB manufacturing for high production rates.

In Figure 4b, a wiring strip is attached using the magnetic cores for alignment, constraining the corrugation hinges and supplying soldered electrical connection to

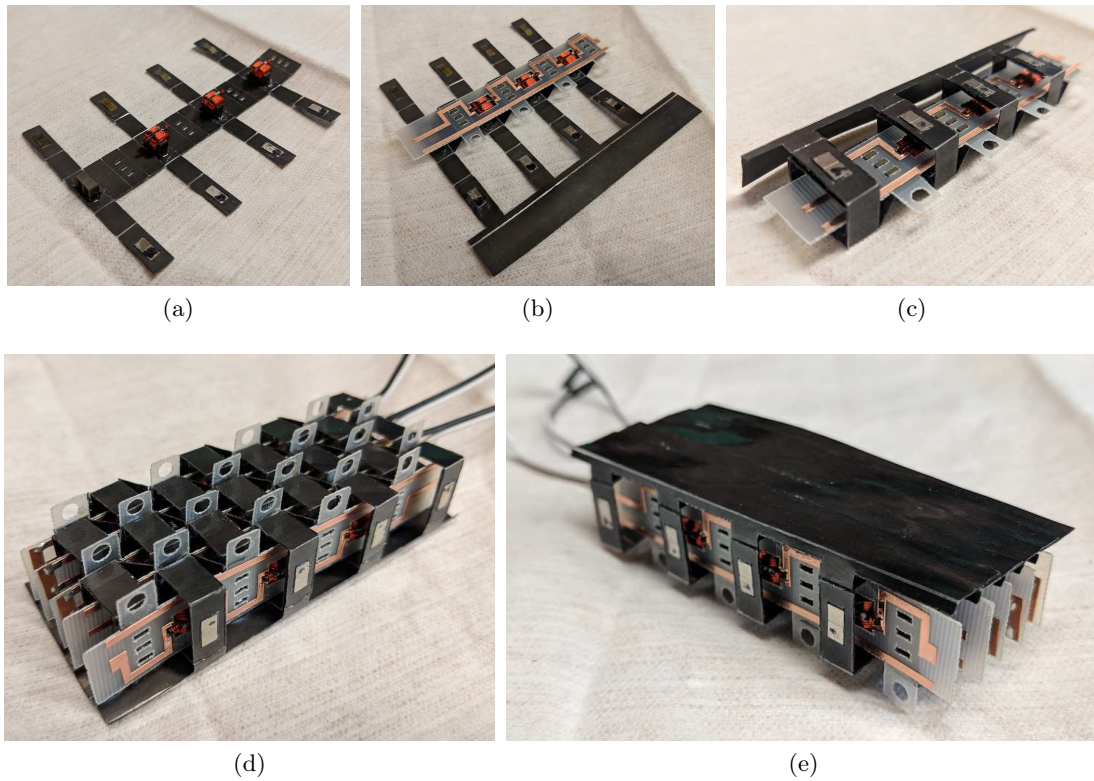


Figure 4: Assembly steps. A) Populate wound cores, magnets, and back-iron components, B) Apply electrical routing and skin strips to constrain corrugation hinge angles, C) Bring magnets and back-iron components together to complete flexure bearing, D) Multiple row units are stacked, E) Skin strips lap and are joined into a continuous aerodynamic skin.

the motors. The wiring strips are produced using a simplified flex-PCB manufacturing process, where adhesive-backed copper foil is kiss-cut and transferred to 125um Garolite G10. The copper traces are optically registered, and additional features and an outline are cut. Again, while soldering was performed manually, this is amenable to reflow or wave soldering such as is used in industrial PCB manufacturing. At this stage, a skin strip is attached with cyanoacrylate glue, using magnet edges for registration. These skin strips are made with the same fiber-reinforced composite process described above, but with an overall thickness of roughly 100um.

In Figure 4c, the magnets and back-iron components are brought together with the aid of attractive forces, assembling the flexure bearings for the linear motors. This connection is strengthened with cyanoacrylate glue, completing the assembly of a full strip unit. Multiple units can be assembled to create a honeycomb with embedded linear actuators. The stator of one unit aligns with the rotor of an adjacent unit, loading the flexure bearings in tension and setting a consistent air gap (roughly 800 um in the prototype shown in Figure 4). The skin strips of each row overlap slightly with that of the adjacent row. These skins are bonded and covered with adhesive-backed PET (50um thickness) to create a smooth hydrodynamic surface.

## 4 Characterization

This section describes characterization work to ensure the produced force and frequencies meet the requirements of a hydrodynamic traveling wave application.



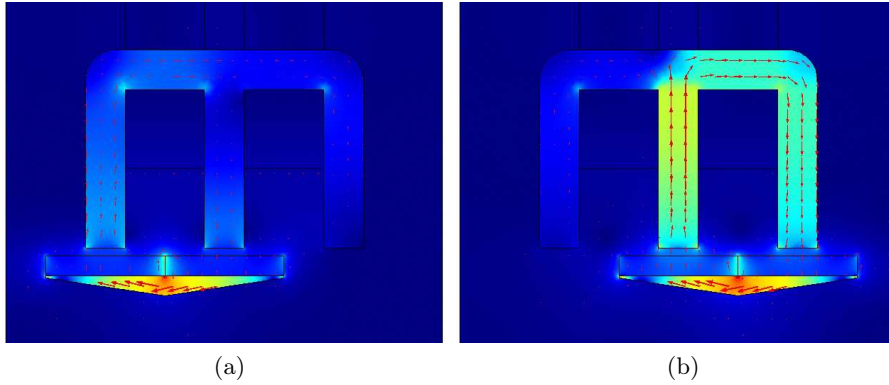


Figure 5: Simulated flux intensity (colormap) and direction (arrows) under positive current of 1 amp. A) A negative most stroke limit, B) At positive most stroke limit.

#### 4.1 Force

To evaluate force produced by the linear motors, we compare finite element simulation and experimental testing. The simulations were performed using COMSOL Multiphysics [13]. Figure 5 shows one simulation, with flux intensity and direction drawn for a linear motor in minimum (5a) and maximum (5b) configurations of the stroke when the phase current is one ampere. In Figure 5a, the field of the permanent magnets opposes the field produced by the coils, and flux seeks alternate paths than the iron core. In Figure 5b, the two flux distributions are aligned, providing a low reluctance magnetic circuit through the core. To simulate these effects, we assumed a planar flux distribution and ran a two-dimensional simulation, significantly lowering the computational burden. While the flux distributions are largely planar, this neglects fringing fields. Thus we expect simulations to slightly overestimate force produced but roughly preserve dependence on geometric parameters.

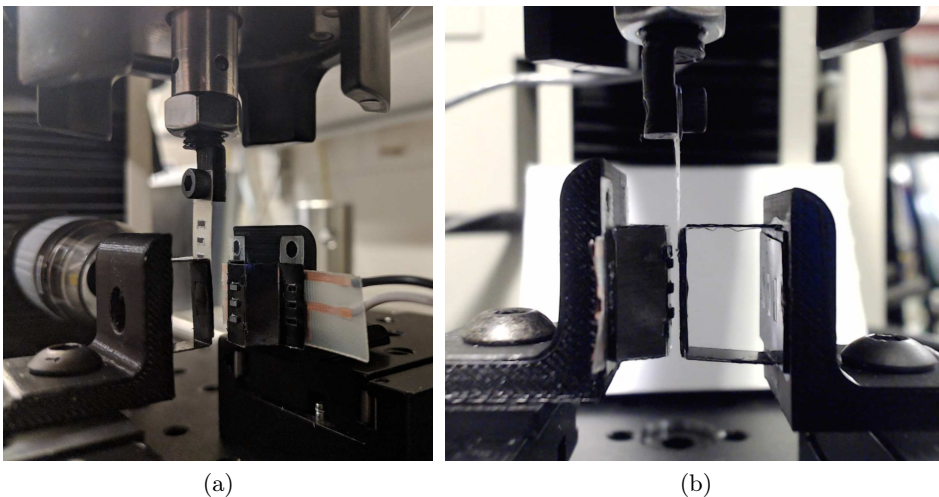


Figure 6: Test setup for force measurement on material characterization machine. A) Perspective view, showing 5N load cell, flexure for transmitting force, linear stages, and power wiring. B) Side view, showing prescribed gap between magnetic core and magnets.

We simulated flux distributions and resulting force on the rotor for a range of coil currents, stroke positions, and core geometries. These studies indicated the size

of the back-iron was significant in increasing actuator force but also in the moving mass. For these reasons, we designed the triangular back-iron shown in Figure 5, which limits magnetic saturation while avoiding unnecessary moving mass.

To compare simulated values with our physical prototypes, we measured force using a materials characterization machine (Instron 4411) with 5 N load cell, shown in Figure 6. We used linear slides to precisely position the rotor and stator and transmitted force to the load cell using a Garolite flexure to avoid off-axis loads.

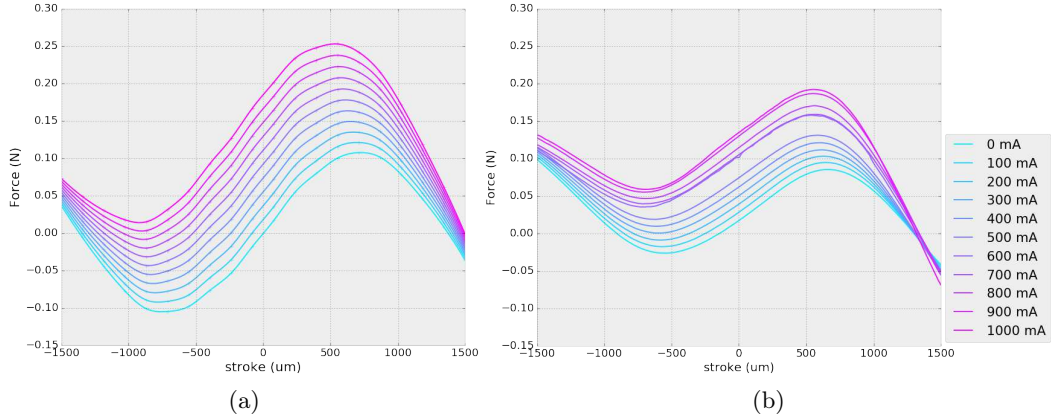


Figure 7: A) Two-dimensional simulation and B) measured force with 800um air gap.

Figure 7 plots force vs. stroke and current for simulated and measured actuators with an 800um air gap. Deviations from a planar flux distribution are responsible for roughly 20% reduction in peak force at 1 ampere phase current. We note that 800um is a conservative air gap, selected because smaller air gaps deformed rotor flexure under attractive forces. With a stiffer rotor, smaller air gaps could increase force without significantly increasing moving mass. Despite this, the force magnitudes comfortably exceed the fluid mechanical requirements derived in Section 2.

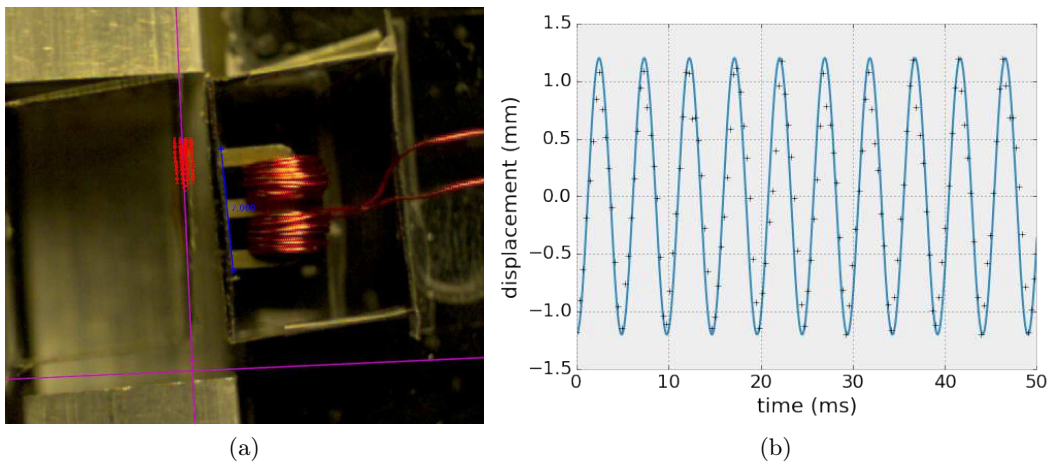


Figure 8: 200 Hz operation: A) Video with motion tracking, B) Extracted trajectory.

## 4.2 Frequency

To characterize the high frequency operation of our actuators, we performed simple trials with square wave drive inputs of varying frequency using a single actuator

with no skin attached. In a fully assembled honeycomb, the rotor travel is limited by the adjacent strip units, but to test variable travel limits, we implemented physical end stops using aluminum bars in these high frequency trials.

Figure 8 shows the results of sending a 200 Hz driving frequency to the actuator with a current limit of approximately 1 ampere. The resulting trajectory was recorded using a high speed video camera (Krontech Chronos 1.4) at 3000 frames per second. We used video tracking software (Physlets Tracker) to extract the trajectory and plot it in Figure 8b. This simple test shows that our actuator is capable of driving its rotor at 200 Hz with an amplitude of approximately 1.2mm.

## 5 Conclusions

We detailed a candidate system for fabricating foils with driven traveling surface waves. Studies suggest that traveling waves can eliminate separation and significantly reduce drag if wave speed moderately exceeds free stream speed, but building physical prototypes meeting these requirements has proven difficult. The origami-inspired manufacturing techniques described above produce structures with embedded actuation, motion guides, wiring, and structural support that may realize this engineering challenge.

In this work, we first estimated wave parameters based on hydrodynamics and developed a specification for force, frequency, and size required of an actuator system. We described a generalizable method for producing fiber-reinforced panels with prescribed hinge lines, which when populated with electromagnetic components produce shaped volumes with embedded actuators for driving surface waves. We then simulated and measured performance of our actuation system in force and frequency. In both metrics, performance showed a safe margin over stated requirements.

With these encouraging preliminary results, there is considerable future work that can improve this distributed actuation system. First, the performance testing described above was carried out on the level of a single actuator without the contribution of bending stiffness of a skin and the interactions between adjacent actuator rows. Using fiber alignment and hinge placement, the skin strips in this work were designed to have much lower bending stiffness in the chordwise direction than in the spanwise direction. This minimizes the actuator work required to overcome bending stiffness, but this must be tested. Future work must also address the necessary compliance in mounting skin panels to accommodate the chordwise geometric effects of the wave amplitude without causing binding of the rotor flexure bearings.

It is expected that future work could considerably improve actuator performance. As mentioned, the air gap used in measurements was conservative due to deformation of the rotor under smaller air gaps. By stiffening the rotor, smaller gaps can be used, increasing generated force without significantly increasing moving mass. Further, the drive signals used were simple current-controlled voltage square waves. Better control would use the actuator transfer function to increase average force generated while maintaining safe thermal dissipation (the effective limit on driving current).

Finally, an obvious next step is to experimentally verify that the hydrodynamic performance characteristics can be realized and test hypotheses about traveling waves. If successful, the macroscopic drag reduction effects of traveling waves could be measured with a load cell, while the elimination of separation and wave-scale phenomena could be visualized using PIV or other flow visualization techniques. This exciting work is currently an active research effort.

## Acknowledgements

Sam Calisch and Neil Gershenfeld are supported by the MIT Center for Bits and Atoms research consortia. Gurvan Jodin's contributions are carried out within the Smart Morphing and Sensing project and the EU's H2020 program for research, technological development and demonstration under grant agreement No. 723402. Michael Triantafyllou and Dixia Fan are supported by the MIT Sea Grant program.

## References

- [1] Oluwaseun A Araromi, Conor J Walsh, and Robert J Wood. Hybrid carbon fiber-textile compliant force sensors for high-load sensing in soft exosuits. In *Intelligent Robots and Systems (IROS), 2017 IEEE/RSJ International Conference on*, pages 1798–1803. IEEE, 2017.
- [2] Remo Brühwiler, Benjamin Goldberg, Neel Doshi, Onur Ozcan, Noah Jafferis, Michael Karpelson, and Robert J Wood. Feedback control of a legged microrobot with on-board sensing. In *Intelligent Robots and Systems (IROS), 2015 IEEE/RSJ International Conference on*, pages 5727–5733. IEEE, 2015.
- [3] Sam Calisch and Neil Gershenfeld. Kirigami fabrication of shaped, flat-foldable cellular materials based on the tachi-miura polyhedron. *7OSME*, In Review, 2018.
- [4] Sam Calisch and Neil Gershenfeld. Towards continuous production of shaped honeycombs. In *ASME 2018 Manufacturing Science and Engineering Conference*. American Society of Mechanical Engineers, 2018.
- [5] Wenli Chen, Yang Liu, Feng Xu, Hui Li, and Hui Hu. *Suppression of Vortex Shedding from a Circular Cylinder by using a Traveling Wave Wall*. American Institute of Aeronautics and Astronautics, 2018/01/15 2014.
- [6] Mihai Duduta, David R Clarke, and Robert J Wood. A high speed soft robot based on dielectric elastomer actuators. In *Robotics and Automation (ICRA), 2017 IEEE International Conference on*, pages 4346–4351. IEEE, 2017.
- [7] Maryam Eidini and Glaucio H. Paulino. Unraveling metamaterial properties in zigzag-base folded sheets. *Science Advances*, 1(8), 2015.
- [8] S. Felton, M. Tolley, E. Demaine, D. Rus, and R. Wood. A method for building self-folding machines. *Science*, 345(6197):644–646, 2014.
- [9] SM Felton, KP Becker, DM Aukes, and RJ Wood. Self-folding with shape memory composites at the millimeter scale. *Journal of Micromechanics and Microengineering*, 25(8):085004, 2015.
- [10] Evgueni T. Filipov, Tomohiro Tachi, and Glaucio H. Paulino. Origami tubes assembled into stiff, yet reconfigurable structures and metamaterials. *Proceedings of the National Academy of Sciences*, 112(40):12321–12326, 2015.
- [11] Benjamin Goldberg, Michael Karpelson, Onur Ozcan, and Robert J Wood. Planar fabrication of a mesoscale voice coil actuator. In *Robotics and Automation (ICRA), 2014 IEEE International Conference on*, pages 6319–6325. IEEE, 2014.
- [12] Sebastian Heimbs. Foldcore sandwich structures and their impact behaviour: an overview. In *Dynamic failure of composite and sandwich structures*, pages 491–544. Springer, 2013.
- [13] COMSOL Inc. Comsol multiphysics reference manual, version 5.3. [www.comsol.com](http://www.comsol.com).
- [14] Noah T Jafferis, Mario Lok, Nastasia Winey, Gu-Yeon Wei, and Robert J Wood. Multilayer laminated piezoelectric bending actuators: design and manufacturing for optimum power density and efficiency. *Smart Materials and Structures*, 25(5):055033, 2016.
- [15] Kaushik Jayaram, Noah Thomas Jafferis, Neel Doshi, Benjamin Goldberg, and Robert J Wood. Concomitant sensing and actuation for piezoelectric microrobots. *Smart Materials and Structures*, 2018.
- [16] Shuguang Li, Daniel M Vogt, Daniela Rus, and Robert J Wood. Fluid-driven origami-inspired artificial muscles. *Proceedings of the National Academy of Sciences*, page 201713450, 2017.
- [17] Kevin Y. Ma, Pakpong Chirarattananon, Sawyer B. Fuller, and Robert J. Wood. Controlled flight of a biologically inspired, insect-scale robot. *Science*, 340(6132):603–607, 2013.

- [18] Kevin Y Ma, Pakpong Chirarattananon, and Robert J Wood. Design and fabrication of an insect-scale flying robot for control autonomy. In *Intelligent Robots and Systems (IROS), 2015 IEEE/RSJ International Conference on*, pages 1558–1564. IEEE, 2015.
- [19] Ronit Malka, Alexis Lussier Desbiens, Yufeng Chen, and Robert J Wood. Principles of microscale flexure hinge design for enhanced endurance. In *Intelligent Robots and Systems (IROS 2014), 2014 IEEE/RSJ International Conference on*, pages 2879–2885. IEEE, 2014.
- [20] Hayley McClintock, Fatma Zeynep Temel, Neel Doshi, Je-sung Koh, and Robert J Wood. The millidelta: A high-bandwidth, high-precision, millimeter-scale delta robot. *Science Robotics*, 3(14):eaar3018, 2018.
- [21] Robin M. Neville, Fabrizio Scarpa, and Alberto Pirrera. Shape morphing kirigami mechanical metamaterials. *Scientific Reports*, 6:31067 EP –, 08 2016.
- [22] Taketoshi Nojima and Kazuya Saito. Development of newly designed ultra-light core structures. *JSME International Journal Series A Solid Mechanics and Material Engineering*, 49(1):38–42, 2006.
- [23] Cagdas D Onal, Michael T Tolley, Robert J Wood, and Daniela Rus. Origami-inspired printed robots. *IEEE/ASME transactions on mechatronics*, 20(5):2214–2221, 2015.
- [24] Cagdas D Onal, Robert J Wood, and Daniela Rus. Towards printable robotics: Origami-inspired planar fabrication of three-dimensional mechanisms. In *Robotics and Automation (ICRA), 2011 IEEE International Conference on*, pages 4608–4613. IEEE, 2011.
- [25] Jochen Pflug. Coretinium®: a new tata steel material based on econcore’s innovative thermhex technology. *Reinforced Plastics*, 60(2):107 – 109, 2016.
- [26] Jochen Pflug, B Vangrimde, Ignace Verpoest, Dirk Vandepitte, M Britzke, and A Wagenführ. Continuously produced paper honeycomb sandwich panels for furniture applications. In *5th Global Wood and Natural Fibre Composites Symposium. Kassel, Germany, April*, pages 27–28, 2004.
- [27] Jochen Pflug, Bart Vangrimde, Ignace Verpoest, Philipp Bratfisch, and Dirk Vandepitte. Honeycomb core materials: New concepts for continuous production of honeycomb core materials. *Sampe journal*, 39(6):22–30, 2003.
- [28] Kazuya Saito, Sergio Pellegrino, and Taketoshi Nojima. Manufacture of arbitrary cross-section composite honeycomb cores based on origami techniques. *Journal of Mechanical Design*, 136(5):051011, 2014.
- [29] Lian Shen, Xiang Zhang, Dick KP Yue, and Michael S Triantafyllou. Turbulent flow over a flexible wall undergoing a streamwise travelling wave motion. *Journal of Fluid Mechanics*, 484:197–221, 2003.
- [30] ByungHyun Shin, Samuel M Felton, Michael T Tolley, and Robert J Wood. Self-assembling sensors for printable machines. In *Robotics and Automation (ICRA), 2014 IEEE International Conference on*, pages 4417–4422. IEEE, 2014.
- [31] Xu Sun, Samuel M Felton, Robert J Wood, and Sangbae Kim. Printing angle sensors for foldable robots. In *Intelligent Robots and Systems (IROS), 2015 IEEE/RSJ International Conference on*, pages 1725–1731. IEEE, 2015.
- [32] MS Triantafyllou, FS Hover, AH Tchet, and DK Yue. Review of hydrodynamic scaling laws in aquatic locomotion and fishlike swimming. *Applied Mechanics Reviews*, 58(4):226–237, 2005.
- [33] Lijun Wang, Kazuya Saito, You Gotou, and Yoji Okabe. Design and fabrication of aluminum honeycomb structures based on origami technology. *Journal of Sandwich Structures & Materials*, 0(0):1099636217714646, 2017.
- [34] Robert J Wood, Srinath Avadhanula, Ranjana Sahai, Erik Steltz, and Ronald S Fearing. Microrobot design using fiber reinforced composites. *Journal of Mechanical Design*, 130(5):052304, 2008.
- [35] Chui-Jie Wu, Liang Wang, and Jie-Zhi Wu. Suppression of the von kármán vortex street behind a circular cylinder by a travelling wave generated by a flexible surface. *Journal of Fluid Mechanics*, 574:365–391, 2007.
- [36] Feng Xu, Wen-Li Chen, Wei-Feng Bai, Yi-Qing Xiao, and Jin-Ping Ou. Flow control of the wake vortex street of a circular cylinder by using a traveling wave wall at low reynolds number. *Computers and Fluids*, 145:52 – 67, 2017.
- [37] Yan Yao, Chuan jing Lu, Ting Si, and Kun Zhu. Experimental investigation on the drag reduction characteristics of traveling wavy wall at high reynolds number in wind tunnel. *Journal of Hydrodynamics, Ser. B*, 22(5):719 – 724, 2010.